Laser-Induced Adiabat Shaping by Relaxation in Inertial Confinement Fusion Implosions

Introduction

In direct-drive inertial confinement fusion (ICF), a spherical shell of cryogenic deuterium–tritium is imploded by direct laser irradiation. As the shell accelerates inward, the outer surface is unstable due to the Rayleigh–Taylor (RT) instability, which causes a large shell distortion leading to significant degradation in capsule performance. Controlling the seeds and the growth rates of the RT instability during the acceleration phase is essential for the success of ICF implosions. The main damping mechanism of the instability growth during the acceleration phase is the ablative mass flow[1,2] off the shell's outer surface since the RT growth rates for cryogenic DT can be approximated as[2] $\Gamma \approx 0.94\sqrt{kg} - 2.7\ kV_a$, where g is the shell acceleration, k is the instability wave number, and V_a is the ablation velocity. The latter represents the propagation speed of the heat front into the imploding shell and is inversely proportional to the shell density at the ablation front, $V_a = \dot{m}/\rho_a$, where $\dot{m}$ is the mass ablation rate per unit area and ρ_a is the shell density at the ablation front. While the ablation rate is solely dependent on the laser intensity $\left(\dot{m} \sim I^{1/3}\right)$, the density is related to the local value of the entropy (also referred to as the "adiabat") $\rho_a = \left(p_a/S_a\right)^{1/\gamma}$, where p_a is the ablation pressure, S_a is the ablation-front adiabat, and $\gamma = 5/3$ is the adiabatic index. For a fixed laser wavelength, the ablation pressure depends on the laser intensity $p_a \sim I^{2/3}$, leading to a scaling of the ablation velocity $V_a \sim S_a^{3/5} I^{-1/15}$, which is almost solely dependent on the ablation-front adiabat. The ablation velocity increases for larger values of the adiabat, leading to lower growth rates and improved stability. The 1-D capsule performance degrades, however, as the adiabat increases. Indeed, the energy required for ignition[3] in a 1-D implosion is approximately proportional to S_{dec}^2, and the shell areal density at stagnation decreases for larger S_{dec} (here S_{dec} is the in-flight shell adiabat at the beginning of the deceleration phase).

It is important to emphasize that the 1-D capsule performance is affected by the shell adiabat at the beginning of the deceleration phase (S_{dec}) only when the laser is turned off and mass ablation off the outer shell surface has ceased. Since a large portion of the shell mass is ablated off during the acceleration phase, the 1-D shell performance during the deceleration phase depends on the adiabat of the unablated shell. On the contrary, the ablative stabilization during the acceleration phase depends on the adiabat at the ablation front (S_a), that is, the adiabat of the ablated portion of the shell. It follows that a desirable adiabat shape would exhibit a minimum on the rear surface and a maximum on the ablation front. The idea of adiabat shaping was first introduced in Ref. 4, where the shaping is induced by the interaction of soft x rays with an ablator material having multiple absorption lines and radiation penetration depths. The first target design of such kind[5] makes use of the x rays produced by a thin gold overcoat and by the carbon radiation in a wetted-foam ablator. Even though such a clever design[4,5] can produce the desired shaping, significant complications arise from the target-manufacturing aspect, based on wetted-foam technology.

In this article, we show that it is possible to shape the shell adiabat with only a minor modification of the laser pulse without requiring any change to the shell structure. Adiabat shaping can easily be performed by relaxing the density profile of the shell with a weak laser prepulse followed by a power shutoff. The adiabat is shaped when the main pulse is turned on, driving a strong shock through the relaxed profile. The adiabat profiles are usually steep, leading to a large increase in the ablation velocity. We refer to this technique as relaxation (RX). A good degree of adiabat shaping can also be accomplished by using a strong prepulse driving a very strong shock in the shell. When the laser power is lowered, the shock decays, leaving behind a shaped-adiabat profile. Shaping by a decayed shock (DS) was first proposed in Ref. 6 by Goncharov *et al*. and is described only briefly here for the purpose of comparison. We refer to Ref. 6 for a more detailed description of the DS technique. Instead, we focus our attention primarily on the RX adiabat shaping requiring only a weak prepulse and therefore easily implementable on current laser systems. Another advantage of the RX technique is that the main pulse starts with a high-intensity foot leading to a low contrast ratio for the main pulse laser power, better conversion efficiency, and therefore

more energy on target. Unlike the DS, the RX-induced adiabat shape is not unique and can be tuned by changing the laser prepulse and main pulse. The benefits of RX shaping have also been confirmed by a series of recent simulations by Perkins[7] *et al*. and may also explain the improved stability observed in the simulations of Lindl and Mead.[8] Furthermore, the use of a laser prepulse may also lead to a reduced level of imprinting.[9]

Analysis of Adiabat Shapes

Both the DS and RX techniques require a prepulse (strong and weak, respectively) launching a decaying strong shock in the shell. We assume that the prepulse produces a constant pressure (P_{prep}) of duration (t_{prep}). The strong shock launched by the pressure $p_* = P_{\text{prep}}$ compresses the shell material to a density $\rho_* \simeq 4\,\rho_0$ (here ρ_0 is the initial shell density) and sets the adiabat of the shocked material to a constant value $S_* = p_* \big/ \rho_*^{5/3}$. After the interval t_{prep}, the laser intensity (and therefore the applied ablation pressure) is greatly reduced, causing a rarefaction wave to propagate from the ablation front toward the shock front. We define with $t = 0$ the time corresponding to the end of the prepulse and launching of the rarefaction wave. Since the leading edge of the rarefaction wave travels faster than the shock, the shock front is overtaken by the rarefaction wave at time $t_* \simeq 0.81\,t_{\text{prep}}$ corresponding to an areal density $m_* = t_* \sqrt{\gamma p_* \rho_*}$. After the shock is overtaken by the rarefaction wave ($t > t_*$), both the shock strength and the adiabat of the shocked material decrease. The analysis is greatly simplified by working in the Lagrangian frame of reference and by using the areal density $m = \int_{r_0}^{r} \rho(r', t)\,dr'$ as the spatial coordinate, with r and r_0 representing the position of the fluid elements and the outermost Langrangian point, respectively.

For the DS case, it is important to determine the entropy shape caused by the decaying shock. Using the normalized variables ρ/ρ_*, p/p_*, t/t_*, $u \big/ \sqrt{\gamma p_*/\rho_*}$, and m/m_*, it is easy to show that the equations of motion and the initial and boundary conditions depend only on γ, suggesting that the normalized adiabat $\hat{S} = S/S_*$ is a universal function of $z = m/m_*$ with a shape depending only on γ. It follows that $\hat{S}(z)$ can be determined once and for all from a single one-dimensional simulation. For $\gamma = 5/3$, the normalized adiabat $\alpha \equiv P(\text{Mb}) \big/ 2.18\,\rho\left(g/\text{cm}^3\right)^{5/3}$ is flat for $m < m_*$ and follows approximately a power law for $m > m_*$:

$$\alpha_{m_* < m < m_{\text{sh}}} \approx \alpha_b \left(m_{\text{sh}}/m\right)^{1.3}, \tag{1}$$

where m_{sh} is the total shell areal density and α_b is the rear-surface adiabat that determines the 1-D performance. It is important to notice that while the adiabat shape is independent of the prepulse characteristics, the front-surface adiabat $\alpha_f = \alpha_b \left(m_{\text{sh}}/m_*\right)^{1.3}$ increases by lowering m_*. This can be accomplished by a short, intense prepulse. After the strong prepulse, the standard main pulse immediately follows, driving the shell to the desired implosion velocity.

For the RX case, the prepulse shock is weaker than the DS case, leading to a negligible entropy variation. During the power shutoff, the rarefaction trailing edge expands outward and the shocked material relaxes. Both the pressure and density profiles develop a monotonically increasing profile up to the shock front. The adiabat shaping occurs later in time when the laser is turned on again and the foot of the main pulse starts (see Fig. 94.19 for a typical laser pulse). At this time (t_{foot}) a strong shock is launched and supported by the pressure of the foot of the main pulse (P_{foot}). The shock travels through the relaxed profiles and initially interacts with the low-pressure material of the rarefaction trailing edge. Because of the large pressure ratio before and after the shock front, the shock strength is initially very high and the shell's outer surface is set on a high adiabat. As the shock travels up the pressure (and density) profile, the pressure of the unshocked material increases and the shock strength decreases, leading to a lower adiabat. When the shock driven by the main pulse merges with the shock launched by the prepulse at the shell's rear surface, the adiabat acquires the desired shape with large values on the outer surface and low values on the inner surface.

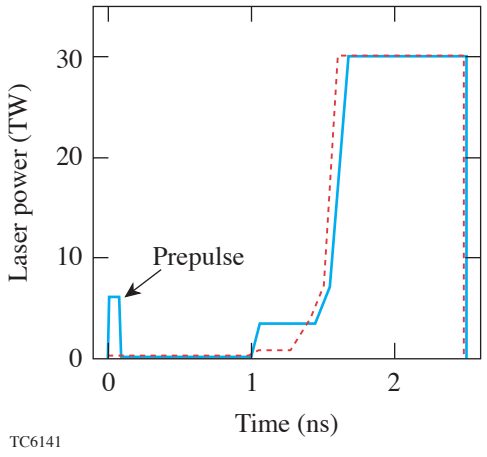

Figure 94.19
Laser pulse for a flat adiabat (dashed) and for adiabat shaping by relaxation (RX) (solid).

The adiabat shape can be calculated analytically for the two limiting cases: (a) a long prepulse launching a rarefaction wave that catches the shock just before the shell's rear surface ($m_* \simeq m_{\rm sh}$) and (b) a short prepulse with a rarefaction wave catching the shock near the front surface ($m_* << m_{\rm sh}$). In case (a), the relaxed density profile just before the main shock launch follows a power law of the areal density $\rho \sim m^{0.75}$. The propagation of the main shock through such a profile can be calculated analytically, leading to the following entropy profile after the main shock:

$$\alpha \approx \alpha_b \left(m_{\rm sh}/m\right)^{1.25}. \tag{2}$$

Observe that the adiabat shape follows a power law similar to the decaying shock case [Eq. (1)] except for the absence of the flat-adiabat region for $m < m_*$, therefore extending the large adiabat profile through the entire shell. In case (b), the relaxed density profile just before the main shock can also be approximated with a power law of the areal density but with a higher exponent $\rho \sim m^{1.45}$ for $m > m_*$ (here $m_* << m_{\rm sh}$). When the exponent exceeds unity, the hydro equations for the main shock propagation cannot be solved exactly. Instead, an approximate solution can be found by assuming that the pressure profile behind the shock is linear in the areal density. A straightforward manipulation of the hydro equations leads to the following adiabat shape behind the main shock:

$$\alpha = \alpha_b \left(\frac{m_{\rm sh}}{m}\right)^{2.4} \frac{1+\Theta\left(m/m_*\right)}{1+\Theta\left(m_{\rm sh}/m_*\right)}, \tag{3}$$

$$\Theta(\xi) = \frac{2.64\,\xi^2 - 8.1\,\xi^{1.45} + 6.4\,\xi - 1}{\left(1-\xi\right)^2}.$$

Observe that the adiabat profile given by Eq. (3) approaches the power law $\alpha \sim m^{-2.4}$ for $m_* \to 0$ and is quite steeper than the one produced by the decaying shock [Eq. (1)], leading to larger values of the adiabat at the ablation front and larger ablation velocities.

Prepulse Design Formulas

The shock-merging condition on the rear surface is a necessary condition for an optimum RX shaping. Indeed, it is easy to show that when the two shocks (main and prepulse) merge inside the shell, the transmitted shock sets the rear surface on an adiabat that is about five times larger than the desired value. Furthermore, if the prepulse shock reaches the rear surface before the main shock, then the back of the shell relaxes and the main shock travels through a decreasing pressure profile, acquiring strength and setting the rear surface on a very high adiabat. The condition of shock merging on the rear surface is an important constraint for a successful adiabat shaping. Assigning the rear-surface adiabat and satisfying the shock-merging requirement are the two conditions needed to determine the starting time and the intensity (i.e., pressure) of the foot of the main laser pulse. A dimensional analysis indicates that four dimensionless parameters can be identified: $\hat{T} = t_{\rm foot}/t_{\rm prep}$, $\hat{P} = P_{\rm foot}/P_{\rm prep}$, $\hat{m} = m_*/m_{\rm sh}$, and $\hat{S} = S_*/S_b$, where $S_* = p_*/\rho_*^{5/3}$ and the $*$ indicates the prepulse hydrodynamic variables. Using the two constraints and a set of numerical simulations in the strong shock regime with different prepulse durations and prepulse pressures, we have constructed a power-law relation among the dimensionless parameters ($\hat{P} \sim \hat{m}^{0.26}\hat{S}^{0.95}$ and $\hat{T} \sim \hat{S}^{0.08}/\hat{m}^{1.76}$), leading to the following simple formulas:

$$P_{\rm foot}^{\rm Mb} \approx 22.5 \left[\frac{100}{\Delta_{\rm sh}^{\mu\rm m}}\right]^{0.26} \left(\frac{\alpha_b}{3}\right)^{0.95} \left[\frac{t_{\rm prep}^{\rm ns}}{0.1}\right]^{0.26} \left[\frac{P_{\rm prep}^{\rm Mb}}{10}\right]^{0.18} \left[\frac{\rho_0^{\rm g/cm^3}}{0.25}\right]^{1.45},$$

$$t_{\rm foot}^{\rm ns} \approx 2.5 \left[\frac{\Delta_{\rm sh}^{\mu\rm m}}{100}\right]^{1.76} \left(\frac{\alpha_b}{3}\right)^{0.08} \left[\frac{0.1}{t_{\rm prep}^{\rm ns}}\right]^{0.76} \left[\frac{10}{P_{\rm prep}^{\rm Mb}}\right]^{0.96} \left[\frac{\rho_0^{\rm g/cm^3}}{0.25}\right]. \tag{4}$$

Observe that the prepulse characteristics can be arbitrarily chosen. For a given prepulse ($P_{\rm prep}$ and $t_{\rm prep}$) and assigned shell thickness $\Delta_{\rm sh}$, density, and rear-surface adiabat (α_b), Eqs. (4) yield the starting time and initial intensity of the foot of the main pulse to within 20%.

Rayleigh–Taylor Growth Rates

1. Analytic Results

The growth rates Γ of the ablative RT in the presence of finite shell entropy gradients can be calculated using a sharp boundary approximation[10] that is valid for $kL_s \sim kd >> 1$, where $k = \ell/R$ is the mode wave number, R is the in-flight radius, d is the target thickness, and $L_s = -S/S'$ is the entropy gradient scale length. The main difference from the standard ablative RT analysis[1,2,10] is in the spatial behavior of the perturbation, which decays slower in the overdense shell as a result of the finite entropy gradient $\tilde{v} \sim \exp\left(-k\hat{h}x\right)$ [instead of the standard exp $(-kx)$], where x is the distance from the ablation front and $\hat{h}$ is the solution to the following transcendental equation:

$$\hat{h}^2 \simeq 1 - \frac{g/\gamma L_s}{\left(\Gamma + k\hat{h}V_a\right)^2} + \frac{1}{\gamma k L_s}. \qquad (5)$$

The last term on the right-hand side is negligible for $kL_s >> 1$. It has been introduced *ad hoc* to recover the growth rates of long wavelengths that are not affected by either ablation or entropy gradients. Observe that the effect of finite entropy gradients *per se* is destabilizing $\left(\hat{h} < 1\right)$; however, the overall effect of adiabat shaping is stabilizing due to the large increase in ablation velocity. In the limit of $kd >> 1$, the RT relation reduces to

$$A\Gamma^2 + B\Gamma k V_a + Ck^2 V_a^2 - D\left(kg - k^2 V_a V_b\right) = 0, \qquad (6)$$

where $A = \hat{h} + \hat{\rho}_b$, $B = \left(1 + \hat{h}\right)^2$, $C = \hat{h}\left(1 + \hat{h}\right)$, and $D = \left(1 - \hat{\rho}_b\right)$ with V_b and $\hat{\rho}_b$ representing the blowoff velocity and normalized density as defined in Eq. (6) of Ref. 2. Equations (5) and (6) must be solved simultaneously to determine the growth rate. It is important to note that an additional instability develops for finite L_s. This is a convective instability driven by the entropy gradients. The convective mode is internal to the shell and poses a serious threat to shell stability only when it grows sufficiently fast and develops the eigenfunction of a wide vortex stretching over a large portion of the shell. Its growth is typically much slower than the RT growth except for short wavelengths when $\Gamma \to \sqrt{g/\gamma L_s}$. Two-dimensional simulations (below) have indicated, however, that this mode grows to a very low amplitude simply because wide vortices are not seeded in the short-wavelength regime. Nevertheless, it is important to investigate the growth of the convective mode on a case-by-case basis since some target designs with extreme adiabat shaping may develop stronger convective instabilities.

2. Simulation Results

The results above are applied to a typical OMEGA cryogenic shell with an inner radius of 345 μm and a DT-ice layer of 85 μm. The shell is driven by a 30-kJ laser pulse (dashed curve in Fig. 94.19) yielding approximately 5.4×10^{14} neutrons on a flat, $\alpha \simeq 3$ adiabat according to a one-dimensional simulation performed with the code *DRACO*.[11] We apply adiabat shaping to the same shell through relaxation, keeping $\alpha_b \simeq 3$ on the rear surface. We use an 85-ps square prepulse with a pressure of 20 Mb and derive the corresponding main-pulse time and foot pressure from Eq. (4), yielding $P_{\text{foot}} \approx$ 25 Mb and $t_{\text{foot}} \approx 1.2$ ns. The pulse in Fig. 94.19 (solid) shows approximately such characteristics when simulated with *DRACO*. The resulting shaped adiabat is shown in Fig. 94.20 (solid) and compared with the theoretical predictions (dotted) from Eq. (3). The 1-D performances of the flat- and shaped-adiabat implosions in terms of yield and peak areal density are within 30% and 7%, respectively. The ablation velocity during the flattop portion of the laser pulse is shown in Fig. 94.21 indicating that the shaped-adiabat implosion exhibits a considerably larger ablation velocity. Figure 94.22 shows the reduction in growth rate versus the mode number ℓ, as given by a series of 2-D *DRACO* simulations. The growth rates are calculated toward the end of the laser flattop when the growth is clearly exponential. Figure 94.22 also shows a comparison with the theoretical growth rates from Eqs. (5) and (6) calculated with 1-D average values obtained from *DRACO*: $\langle g \rangle \simeq 345$ μm/ns^2 and $\langle V_a \rangle \simeq 4.2$ μm/ns^2 for the flat adiabat, and $\langle g \rangle \simeq 345$ μm/ns^2, $\langle V_a \rangle \simeq 6.4$ μm/ns and $L_s \simeq 6$ μm for the

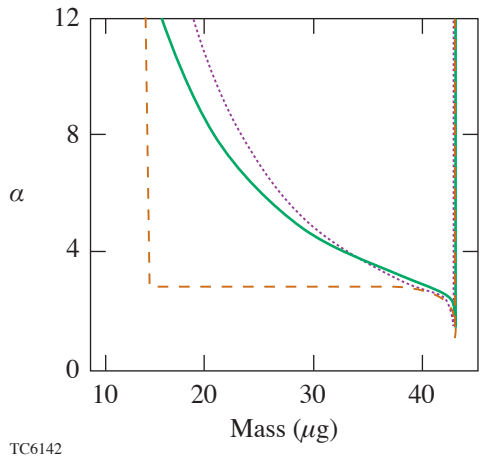

Figure 94.20
Flat adiabat (dashed) and shaped adiabat (solid) profiles induced by the pulses of Fig. 94.19. The dotted curve is the result of Eq. (3).

shaped adiabat. The large reduction in growth rates induced by the high ablation velocity indicates that adiabat shaping can significantly improve the stability of imploding shells.

The anomalous behavior of the growth rate in modes $\ell \sim 200$ shown in Fig. 94.22 is due to a resonant interaction of the RT mode with the convective mode. When the vorticities of the convective and RT modes have the same sign, they add constructively, thereby amplifying the growth rate of the surface perturbation. Figure 94.23 shows radial lineouts of the vorticity for the shaped mode $\ell = 200$ case at two times. The first snapshot (a) is at the beginning of the convective–RT interaction. One can clearly see the RT mode at the ablation front and a larger amplitude convective mode just inside the ablation front. The second snapshot (200 ps later) shows a significant amplification of the RT vorticity as the ablation surface penetrates into the convective cell. This interaction occurs to varying extents at modes of all wavelengths; however, it is most noticeable in regimes where neither mode dominates. Note that under the right circumstance, this convective–RT

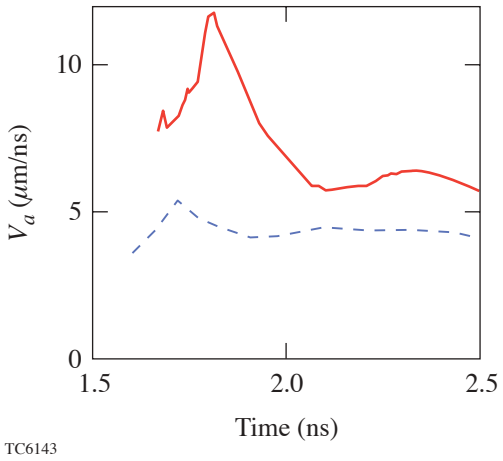

Figure 94.21
Time evolution of the ablation velocities during the power flattop for the flat-adiabat (dashed) and shaped-adiabat (solid) implosions.

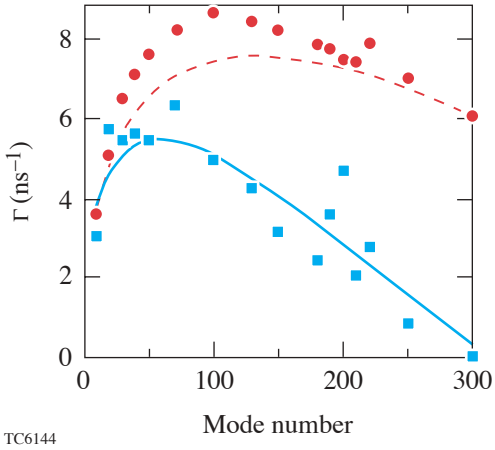

Figure 94.22
RT growth rates versus mode number ℓ for the flat adiabat from *DRACO* (circles) and from Eqs. (5) and (6) (dashed) and for the shaped adiabat from *DRACO* (squares) and from Eqs. (5) and (6) (solid).

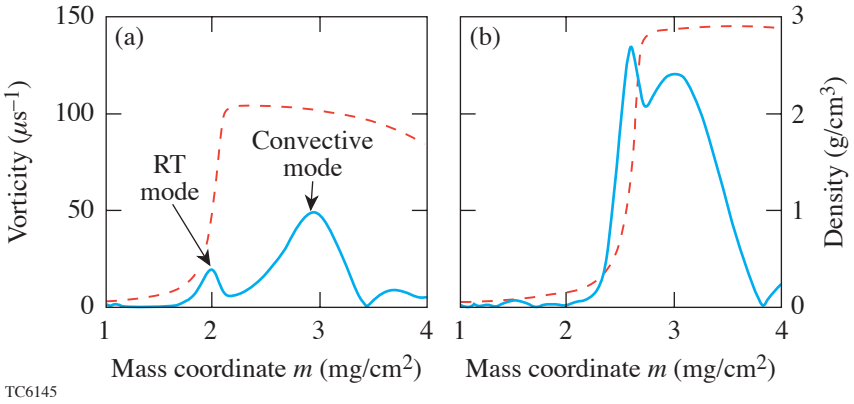

Figure 94.23
Vorticity (solid line) and density (dashed line) for the shaped-adiabat, $\ell = 200$ case (a) at the beginning of the convective–RT mode interaction and (b) 200 ps later.

interaction may also be destructive, leading to lower-than-expected growth rates.

We have developed the theoretical basis (adiabat profiles, laser pulses, RT-growth rates) for laser-induced adiabat shaping by relaxation and have shown that RT growth rates can be reduced without significantly degrading 1-D capsule performances.

ACKNOWLEDGMENT

The authors would like to thank Profs. V. Goncharov and J. Sanz for many useful discussions on adiabat shaping and ablative RT. This work was supported by the U.S. Department of Energy Office of Inertial Confinement Fusion under Cooperative Agreement No. DE-FC03-92SF19460, the University of Rochester, and the New York State Energy Research and Development Authority. The support of DOE does not constitute an endorsement by DOE of the views in this article.

REFERENCES

1. S. E. Bodner, Phys. Rev. Lett. **33**, 761 (1974); H. Takabe *et al.*, Phys. Fluids **28**, 3676 (1985); J. Sanz, Phys. Rev. Lett. **73**, 2700 (1994).

2. R. Betti, V. N. Goncharov, R. L. McCrory, and C. P. Verdon, Phys. Plasmas **5**, 1446 (1998).

3. M. C. Herrmann, M. Tabak, and J. D. Lindl, Nucl. Fusion **41**, 99 (2001); A. Kemp, J. Meyer-ter-Vehn, and S. Atzeni, Phys. Rev. Lett. **86**, 3336 (2001); R. Betti, K. Anderson, V. N. Goncharov, R. L. McCrory, D. D. Meyerhofer, S. Skupsky, and R. P. J. Town, Phys. Plasmas **9**, 2277 (2002).

4. J. H. Gardner, S. E. Bodner, and J. P. Dahlburg, Phys. Fluids B **3**, 1070 (1991).

5. S. E. Bodner *et al.*, Phys. Plasmas **7**, 2298 (2000); L. Phillips *et al.*, Laser Part. Beams **17**, 225 (1999).

6. V. N. Goncharov, "Improved Performance of Direct-Drive ICF Target Designs with Adiabat Shaping Using an Intensity Picket," to be published in Physics of Plasmas.

7. L. J. Perkins, M. Tabak, J. Lindl, D. Bailey, J. Harte, A. Schmitt, S. Obenschain, and R. Betti, Bull. Am. Phys. Soc. **47**, 101 (2002).

8. J. D. Lindl and W. C. Mead, Phys. Rev. Lett. **34**, 1273 (1975).

9. T. J. B. Collins and S. Skupsky, Phys. Plasmas **9**, 275 (2002).

10. A. R. Piriz, J. Sanz, and L. F. Ibañez, Phys. Plasmas **4**, 1117 (1997).

11. D. Keller, T. J. B. Collins, J. A. Delettrez, P. W. McKenty, P. B. Radha, B. Whitney, and G. A. Moses, Bull. Am. Phys. Soc. **44**, 37 (1999).